Effect of hyperfine interactions on ultracold molecular collisions: NH($^3\Sigma^-$) with Mg(^{1}S) in magnetic fields

Maykel L. González-Martínez and Jeremy M. Hutson
Department of Chemistry, Durham University, Durham DH1 3LE, United Kingdom
(Received 23 August 2011; published 7 November 2011)

We investigate the effect of hyperfine interactions on ultracold molecular collisions in magnetic fields, using ^{24}Mg(^1S)+^{14}NH($^3\Sigma^-$) as a prototype system. We explore the energy and magnetic-field dependence of the cross sections, comparing the results with previous calculations that neglected hyperfine interactions [A.O.G. Wallis and J. M. Hutson, Phys. Rev. Lett. **103**, 183201 (2009)]. The main effect of hyperfine interactions for spin relaxation cross sections is that the kinetic energy release of the dominant outgoing channels does not reduce to zero at low fields. This results in reduced centrifugal suppression of the cross sections and increased inelastic cross sections at low energy and low field. We also analyze state-to-state cross sections, for various initial states, and show that hyperfine interactions introduce additional mechanisms for spin relaxation. In particular, there are hyperfine-mediated collisions to outgoing channels that are not centrifugally suppressed. However, for Mg + NH these unsuppressed channels make only small contributions to the total cross sections. We consider the implications of our results for sympathetic cooling of NH by Mg and conclude that the ratio of elastic to inelastic cross sections remains high enough for sympathetic cooling to proceed.

DOI: 10.1103/PhysRevA.84.052706 PACS number(s): 34.50.Cx, 33.15.Pw, 37.10.Mn, 37.10.Pq

I. INTRODUCTION

High-density samples of cold ($T < 1$ K) and ultracold ($T < 1$ μK) molecules are likely to have important applications in fields including quantum information science, high-precision spectroscopy, and quantum-controlled chemistry [1]. For nearly three decades, ultracold atoms have been produced using laser Doppler cooling and evaporative cooling. At temperatures between 1 nK and 1 μK, atoms enter a fully quantal regime with novel properties, forming Bose-Einstein condensates [2–4] and Fermi-degenerate gases [5,6]. However, cooling molecular samples to the temperatures required for quantum degeneracy is much more difficult than for atoms, because molecules have a much richer internal structure.

Molecular cooling techniques can be classified as either *direct* or *indirect*. In direct methods, molecules are cooled from relatively high temperatures by techniques such as buffer-gas cooling [7], Stark deceleration [8], or Zeeman deceleration [9–11]. In addition, laser Doppler cooling has very recently been demonstrated for SrF [12], although only a limited number of molecular species are likely to be amenable to this technique. Indirect methods, by contrast, form ultracold molecules in gases of previously cooled atoms by magnetoassociation [13,14] or photoassociation [13,15]. In the last few years, indirect methods in association with stimulated Raman adiabatic passage [16] have succeeded in producing ground-state molecules at temperatures below 1 μK [17–19]. Indirect methods are, however, restricted to molecules formed from the relatively few atomic species that can be laser cooled.

Direct methods can in principle be used for a wide variety of molecules, but the lowest temperatures achieved so far are in the millikelvin regime. A *second-stage* cooling technique is needed to cool molecules down to the microkelvin range, from which evaporative cooling could reach the region of quantum degeneracy. *Sympathetic cooling* is a promising second-stage cooling method, which relies on thermalization of the molecular species of interest by collisions with ultracold atoms. Sympathetic cooling has been used for almost three decades to cool molecular ions to temperatures around 100 mK and below ([20], Chap. 18), and has more recently also been used for neutral atoms [21,22]. Its extension to neutral molecules was first proposed in 2004 by Soldán and Hutson [23]. Since then, accurate quantum scattering calculations have suggested that it should work for a few diatomic [24,25] and polyatomic molecular species [26,27] in combination with appropriate ultracold atoms. Although experimental validation is still needed, there is great hope that sympathetic cooling will eventually become a "routine" second-stage cooling technique, capable of producing large molecular samples in the microkelvin regime, where most of the new interesting applications would become possible [1].

Cold atoms and molecules are usually held in traps formed with electric, magnetic, or optical fields. By far the most experimentally accessible traps are those formed by static electric [28] and magnetic fields [7]. The main limitation of such traps is that they can hold only those molecules whose energy *increases* with applied field, i.e., those in low-field-seeking states. However, there are always untrapped high-field-seeking states that lie energetically below the low-field-seeking states. Inelastic (deexcitation) collisions that transfer molecules to high-field-seeking states therefore lead to trap loss. Elastic collisions, by contrast, are required for thermalization. Thus, the success of both sympathetic and evaporative cooling depends on a favorable ratio of elastic to inelastic cross sections, of at least about 100 [29].

In the (ultra)cold regime, hyperfine interactions are larger than or comparable to the kinetic energies involved. Hyperfine couplings also provide both additional relaxation mechanisms and new ways to control atomic and molecular collisions. However, only a few calculations have so far considered the consequences of hyperfine interactions on cold molecular collisions. Bohn and co-workers considered the scattering of polar ^{16}OH($^2\Pi_{3/2}$) molecules in static electric [30] and magnetic fields [31]. Lara *et al.* [32,33] studied the

field-free scattering of Rb(^2S) and OH($^2\Pi_{3/2}$). Tscherbul *et al.* studied (ultra)cold collisions of YbF($^2\Sigma$) molecules with He in external electric and magnetic fields [34]. They found that simultaneous electron and nuclear spin relaxation for collisions in the ground rotational state can occur through couplings via excited rotational states and hyperfine terms.

In the present paper, we explore the effects of hyperfine interactions on the ultracold scattering of NH with Mg in the presence of a magnetic field. This extends the study in [34] in various ways: (1) NH is a $^3\Sigma$ instead of a $^2\Sigma$ molecule; (2) NH has two nuclei with nonzero spin, leading to more complicated hyperfine structure than for YbF; (3) we consider other hyperfine states in addition to spin-stretched states. Our results are compared with those of a previous study of Mg-NH neglecting hyperfine terms [24], and allow us to make some general conclusions on how hyperfine interactions can affect the prospects of sympathetic cooling.

II. THEORY

We consider the scattering of ^{14}NH($^3\Sigma^-$) molecules with ^{24}Mg(^1S) atoms in the presence of an external magnetic field B, whose direction defines the space-fixed Z axis. The system is described using Jacobi vectors and coordinates: the vector $\boldsymbol{r}$ runs from N to H while $\boldsymbol{R}$ runs from the center of mass of NH to Mg. The angle between $\boldsymbol{r}$ and $\boldsymbol{R}$ is θ. The collision is studied by solving the time-independent Schrödinger equation for the scattering wave function Ψ at energy E, $\hat{\mathcal{H}}\Psi = E\Psi$, where $\hat{\mathcal{H}}$ is the Hamiltonian for the colliding pair.

A. Effective Hamiltonian

By convention, lower-case symbols are used for quantum numbers of the individual monomers, and capital letters for quantum numbers of the collision complex as a whole. Where necessary, the subscripts 1 and 2 refer to Mg and NH, respectively. The diatom is considered to be a rigid rotor in its ground vibrational state. The effective Hamiltonian can be written

$$\hat{\mathcal{H}} = -\frac{\hbar^2}{2\mu}R^{-1}\frac{d^2}{dR^2}R + \frac{\hbar^2\hat{L}^2}{2\mu R^2} + \hat{\mathcal{H}}_{\rm mon} + \hat{\mathcal{H}}_{12}, \qquad (1)$$

where $\hat{L}$ is the space-fixed operator for the end-over-end rotation and μ is the reduced mass of the complex. In general, $\hat{\mathcal{H}}_{\rm mon}$ contains terms describing both isolated monomers, $\hat{\mathcal{H}}_{\rm mon} = \hat{\mathcal{H}}_1 + \hat{\mathcal{H}}_2$. However, ground-state ^{24}Mg has both zero electron spin and zero nuclear spin, so that it contributes only a constant energy, and it is convenient to set $\hat{\mathcal{H}}_1 = 0$. Finally, $\hat{\mathcal{H}}_{12}$ includes all interactions between the monomers, which in the present case reduces to the potential energy surface $\hat{V}(\boldsymbol{u}_r, \boldsymbol{R})$, conveniently expanded in Legendre polynomials,

$$\hat{V}(\boldsymbol{u}_r, \boldsymbol{R}) = \sum_{k=0}^{k_{\rm max}} V_k(r_{\rm eq}, R) P_k(\cos\theta). \qquad (2)$$

Here $\boldsymbol{u}_r$ denotes a unit vector in the direction of $\boldsymbol{r}$, $r_{\rm eq}$ is the equilibrium interatomic distance of NH in its ground vibrational state, and V_k are the radial strength functions. The potential for the Mg-NH system was reported in Ref. [35].

The Hamiltonian for an isolated NH($^3\Sigma^-$) molecule can be written $\hat{\mathcal{H}}_2 = \hat{\mathcal{H}}_{\rm rot} + \hat{\mathcal{H}}_{\rm sn} + \hat{\mathcal{H}}_{\rm ss} + \hat{\mathcal{H}}_{\rm hf} + \hat{\mathcal{H}}_{\rm Z}$. The different terms will be discussed below and correspond, respectively, to the rotational, electron spin-rotation, electron spin-spin, hyperfine, and Zeeman interactions.

If centrifugal distortion and all other higher-order corrections are neglected, the Hamiltonian for the mechanical rotation of NH is $\hat{\mathcal{H}}_{\rm rot} = b_{\rm NH}\hat{n}^2$, where $b_{\rm NH}$ is the rotational constant (with dimensions of energy) and $\hat{n}$ is the operator for the rotational angular momentum. The electron spin-rotation term, arising from the interaction between the magnetic moment associated with the composite electronic spin of NH, $\hat{s}$, and the magnetic field induced by its rotation, can be written $\hat{\mathcal{H}}_{\rm sn} = \gamma\hat{n}\cdot\hat{s}$, where γ is the spin-rotation constant.

The direct dipolar interaction between the unpaired electrons in NH($^3\Sigma^-$) may be written [36]

$$\hat{\mathcal{H}}_{\rm ss} \approx 2\lambda_{\rm ss}{\rm T}^2_{q=0}(\hat{s},\hat{s}){\rm T}^2_{q=0}(\boldsymbol{u}_r,\boldsymbol{u}_r), \qquad (3)$$

where $\lambda_{\rm ss}$ is the electron spin-spin constant and ${\rm T}^k$ represents a spherical tensor of rank k, with q component ${\rm T}^k_q$.

Since both the ^{14}N and ^{1}H nuclei have nonzero nuclear spin, $i_{\rm N} = 1$ and $i_{\rm H} = 1/2$, the hyperfine Hamiltonian can be written

$$\begin{aligned}\hat{\mathcal{H}}_{\rm hf} = {}& \hat{\mathcal{H}}_{\rm si,N} + \hat{\mathcal{H}}_{\rm F,N} + \hat{\mathcal{H}}_{\rm in,N} + \hat{\mathcal{H}}_{\rm Q,N} \\ & + \hat{\mathcal{H}}_{\rm si,H} + \hat{\mathcal{H}}_{\rm F,H} + \hat{\mathcal{H}}_{\rm in,H}. \end{aligned} \qquad (4)$$

Here, $\hat{\mathcal{H}}_{\rm si}$ represents the direct dipolar interaction between the magnetic moments associated with a given nuclear spin $\hat{\imath}$ and the composite electron spin of the open-shell Σ molecule and can be written [36]

$$\begin{aligned}\hat{\mathcal{H}}_{\rm si} &= -\sqrt{10}g_S\mu_{\rm B}g_i\mu_{\rm N}(\mu_0/4\pi){\rm T}^1(\hat{s},\boldsymbol{C}^2)\cdot{\rm T}^1(\hat{\imath}) \\ &\approx \sqrt{6}t_0{\rm T}^2_{q=0}(\hat{s},\hat{\imath}), \end{aligned} \qquad (5)$$

where g_S and g_i are the electron and nuclear g factors, $\mu_{\rm B}$ and $\mu_{\rm N}$ are the Bohr and nuclear magnetons, and μ_0 is the magnetic permeability of free space. The axial dipolar interaction parameter t_0 is related to the widely used constant c defined by Frosch and Foley [37] as $t_0 = c/3$.

The Fermi (or Fermi-Breit) contact interaction $\hat{\mathcal{H}}_{\rm F}$ occurs whenever there is a nonzero electron-spin density at a nucleus with nonzero spin $\hat{\imath}$. It may be written $\hat{\mathcal{H}}_{\rm F} = b_{\rm F}\hat{s}\cdot\hat{\imath}$, where $b_{\rm F}$ is a coupling constant given by $b_{\rm F} = (2/3)g_S\mu_{\rm B}g_i\mu_{\rm N}|\psi(0)|^2$, with $|\psi(0)|^2$ the spin density. The coupling constant can also be written in terms of Frosch and Foley's b and c parameters as $b_{\rm F} = b + (1/3)c$.

Since $i_{\rm N} > 1/2$, the interaction between the nuclear electric quadrupole moment $\boldsymbol{Q}$ and the electric-field gradient at the ^{14}N nucleus, $\nabla\boldsymbol{E}$, must be included. In general, this is [36]

$$\hat{\mathcal{H}}_{\rm Q} = -e{\rm T}^2(\nabla\boldsymbol{E})\cdot{\rm T}^2(\boldsymbol{Q}), \qquad (6)$$

and for a diatomic molecule reduces to

$$\hat{\mathcal{H}}_{\rm Q} = \frac{eq_0Q}{4i(2i-1)}\sqrt{6}{\rm T}^2_{q=0}(\hat{\imath},\hat{\imath}), \qquad (7)$$

where q_0 is the electric-field gradient.

TABLE I. Molecular parameters for ^{14}NH($^3\Sigma^-$,$v = 0$).

Parameter	Value	Reference
$b_{\rm NH}$ (cm^{-1})	16.343	[38]
γ (cm^{-1})	−0.055	[38]
$\lambda_{\rm ss}$ (cm^{-1})	0.92	[38]
$g_{\rm N}$	0.40 376	[39]
$b_{\rm F,N}$ (MHz)	18.83	[40]
$c_{\rm N}$ ($= 3t_{0,\rm N}$) (MHz)	−67.922	[40]
$(eq_0Q)_{\rm N}$ (MHz)	−2.883	[40]
$C_{\rm I,N}$ (MHz)	0.1455	[40]
$g_{\rm H}$	5.58 568	[39]
$b_{\rm F,H}$ (MHz)	−66.131	[40]
$c_{\rm H}$ ($= 3t_{0,\rm H}$) (MHz)	90.291	[40]
$C_{\rm I,H}$ (MHz)	−0.061	[40]

The nuclear spin-rotation terms $\hat{\mathcal{H}}_{\rm in}$ are the nuclear counterpart of the $\hat{\mathcal{H}}_{\rm sn}$ interaction discussed above, and are written $\hat{\mathcal{H}}_{\rm in} = C_{\rm I}\hat{n}\cdot\hat{\imath}$, where $C_{\rm I}$ is the corresponding nuclear spin-rotation constant.

Finally, if only electron and nuclear spin Zeeman terms are taken into account,

$$\hat{\mathcal{H}}_{\rm Z} = g_S\mu_{\rm B}\hat{s}_z\boldsymbol{B} - \mu_{\rm N}\sum_{X={\rm N,H}} g_X\hat{\imath}_{Xz}\boldsymbol{B}(1-\sigma_X). \tag{8}$$

The nuclear shielding factors σ_X are extremely small and are neglected in the present work.

The molecular constants used for the ^{14}NH($^3\Sigma^-$) radical are listed in Table I.

B. Coupled-channel equations

We solve the scattering problem using the coupled-channel method. First, the total wave function is expanded in a set of N conveniently chosen basis functions $|a\rangle$,

$$\Psi(R,\xi) = R^{-1}\sum_a \chi_a(R)|a\rangle. \tag{9}$$

Here, ξ is a collective variable including all coordinates except R, and a is the set of quantum numbers that label our basis functions. Each different combination of quantum numbers a is said to define a *channel*. A set of coupled differential equations for the *channel functions* $\chi_a(R)$ is then obtained by substituting $\Psi(R,\xi)$ into the time-independent Schrödinger equation,

$$\frac{d^2\chi_a}{dR^2} = \sum_{a'}(W_{aa'} - \epsilon\delta_{aa'})\chi_{a'}, \tag{10}$$

where δ_{ij} is the Kronecker delta, $\epsilon = 2\mu E/\hbar^2$ is a scaled energy, and

$$W_{aa'}(R) = \frac{2\mu}{\hbar^2}\langle a|\left[\hat{\mathcal{H}}_{\rm mon} + \hat{\mathcal{H}}_{12} + \frac{\hbar^2\hat{L}^2}{2\mu R^2}\right]|a'\rangle. \tag{11}$$

The coupled equations (10) are solved by propagating a complete set of independent solution vectors from $R_{\rm min}$, deep in the inner classically forbidden region, to $R_{\rm max}$, large enough that the effects of the interaction potential have died off. If necessary, the solutions are transformed at $R_{\rm max}$ into a basis set in which $W_{aa'}$ and $\hat{L}^2$ are diagonal at $R = \infty$ [41], and the transformed channel functions are matched to the standard scattering boundary conditions [42]. This gives the scattering matrix S, from which all quantities of interest, such as state-to-state cross sections and scattering lengths, may be calculated. Numerical details are given in Sec. III B.

C. Basis set and matrix elements

We use a fully uncoupled basis set $|a\rangle \equiv |\alpha\rangle|LM_L\rangle$, where $|\alpha\rangle \equiv |i_{\rm N}m_{i\rm N}\rangle|i_{\rm H}m_{i\rm H}\rangle|sm_s\rangle|nm_n\rangle$ describes the state of the monomers, and m_A (or M_A) denotes the projection on the field axis of the vector operator $\hat{A}$. None of the interactions considered here changes the electronic or nuclear spins, so we omit the labels s and i and label our basis functions $(m_{i\rm N},m_{i\rm H},m_s,n,m_n,L,M_L)$. A static magnetic field conserves both the projection $M_{\rm tot}$ of the total angular momentum F and the total parity P of the system. These are explicitly $M_{\rm tot} = m_{i\rm N} + m_{i\rm H} + m_s + m_n + M_L$ and $P = p_1p_2(-1)^L$, with $p_1 = 1$ the parity of Mg(^1S) and $p_2 = (-1)^{n+1}$ the parity of NH($^3\Sigma^-$). The matrix elements for the centrifugal, rotational, electron spin-spin, and interaction potentials are diagonal in, and independent of, the nuclear spin quantum numbers. The corresponding expressions in our basis set are thus readily obtained from Ref. [41].

The Zeeman matrix elements are completely diagonal in the uncoupled basis set,

$$\begin{aligned}&\langle sm_s|\langle i_{\rm H}m_{i\rm H}|\langle i_{\rm N}m_{i\rm N}|\hat{\mathcal{H}}_{\rm Z}|i_{\rm N}m_{i\rm N}\rangle|i_{\rm H}m_{i\rm H}\rangle|sm_s\rangle\\ &\quad = B[g_S\mu_{\rm B}m_s - \mu_{\rm N}(g_{\rm N}m_{i\rm N} + g_{\rm H}m_{i\rm H})].\end{aligned} \tag{12}$$

Here and throughout this section, the matrix elements are fully diagonal with respect to quantum numbers that do not appear explicitly in the expression.

The Fermi contact term and the electron and nuclear spin-rotation terms all share a similar structure, $\hat{\mathcal{H}}_{j_1j_2} = \kappa\hat{\jmath}_1\cdot\hat{\jmath}_2$, where κ is a scalar while $\hat{\jmath}_1$ and $\hat{\jmath}_2$ are vector operators. In general, their matrix elements in a decoupled basis set $|j_1m_{j1}\rangle|j_2m_{j2}\rangle$ are

$$\begin{aligned}&\langle j_2m_{j2}|\langle j_1m_{j1}|\hat{\mathcal{H}}_{j_1j_2}|j_1m'_{j1}\rangle|j_2m'_{j2}\rangle\\ &\quad = \delta_{m_{j1}m'_{j1}}\delta_{m_{j2}m'_{j2}}\kappa\, m_{j1}m_{j2}\\ &\qquad + \delta_{m_{j1}m'_{j1}\pm1}\delta_{m_{j2}m'_{j2}\mp1}\frac{\kappa}{2}[j_1(j_1+1) - m_{j1}m'_{j1}]^{1/2}\\ &\qquad \times [j_2(j_2+1) - m_{j2}m'_{j2}]^{1/2}.\end{aligned} \tag{13}$$

Such terms can mix functions with adjacent values of the projections of $\hat{\jmath}_1$ and $\hat{\jmath}_2$, but preserve the sum $m_{12} = m_{j1} + m_{j2}$.

The electron-nuclear spin dipolar interaction, Eq. (5), has matrix elements

$$\langle nm_n|\langle sm_s|\langle im_i|\hat{\mathcal{H}}_{\rm si}|im_i'\rangle|sm_s'\rangle|n'm_n'\rangle = t_0\sqrt{30}(-1)^{i-m_i+s-m_s-m_n}[i(i+1)(2i+1)s(s+1)(2s+1)(2n+1)(2n'+1)]^{1/2} \times \begin{pmatrix} n & 2 & n' \\ 0 & 0 & 0 \end{pmatrix} \sum_{q_1,q_2} \begin{pmatrix} 1 & 1 & 2 \\ q_1 & q_2 & -q \end{pmatrix} \begin{pmatrix} i & 1 & i \\ -m_i & q_1 & m_i' \end{pmatrix} \begin{pmatrix} s & 1 & s \\ -m_s & q_2 & m_s' \end{pmatrix} \begin{pmatrix} n & 2 & n' \\ -m_n & -q & m_n' \end{pmatrix}, \tag{14}$$

where $q \equiv q_1 + q_2$ and (:::) is a 3-j symbol. This term produces couplings off-diagonal in one nuclear spin projection m_i, along with m_s and m_n (keeping their sum unchanged), with $\Delta n \equiv n' - n = 0$ or ± 2. This latter selection rule is required to conserve p_2.

Finally, the quadrupole interaction for the ^{14}N nucleus has matrix elements

$$\begin{aligned}\langle nm_n|\langle i_{\rm N}m_{i\rm N}|\hat{\mathcal{H}}_{\rm Q,N}|i_{\rm N}m_{i\rm N}'\rangle|n'm_n'\rangle &= \frac{(eq_0Q)_{\rm N}}{4}(-1)^{i_{\rm N}-m_{i\rm N}-m_n}[(2n+1)(2n'+1)]^{1/2} \\ &\times \begin{pmatrix} n & 2 & n' \\ 0 & 0 & 0 \end{pmatrix} \begin{pmatrix} i_{\rm N} & 2 & i_{\rm N} \\ -i_{\rm N} & 0 & i_{\rm N} \end{pmatrix}^{-1} \\ &\times \sum_p (-1)^p \begin{pmatrix} n & 2 & n' \\ -m_n & p & m_n' \end{pmatrix} \begin{pmatrix} i_{\rm N} & 2 & i_{\rm N} \\ -m_{i\rm N} & -p & m_{i\rm N}' \end{pmatrix}. \end{aligned} \tag{15}$$

These couple functions $\Delta n = 0, \pm 2$ and $\Delta m_{i\rm N} = -\Delta m_n = 0, \pm 1, \pm 2$, thus preserving the sum $m_{i\rm N} + m_n$ as well as p_2.

The first 3-j symbol in Eqs. (14) and (15) implies that the electron-nuclear spin and quadrupolar interactions have no direct off-diagonal matrix elements between $n = 0$ functions, so that their dominant contribution for $n = 0$ is a second-order effect necessarily involving the $n = 2$ excited rotational state; this is also the case for the electron spin-spin interaction.

III. RESULTS AND DISCUSSION

A. Hyperfine levels

The energy levels correlating with the ground rotational state of an isolated ^{14}NH($^3\Sigma^-$) molecule, in an external magnetic field, are shown in Fig. 1. The solid lines correspond to the inclusion of all hyperfine interactions as described in Sec. II A, while the dashed lines show the energy levels obtained when hyperfine terms are neglected.

The hyperfine-free levels are labeled at zero field by the eigenvalues of the angular momentum $\hat{j} = \hat{n} + \hat{s}$, which has only one allowed value, $j = 1$, for $n = 0$ and $s = 1$. In the presence of a magnetic field, a level with quantum number j splits into $2j + 1$ Zeeman components characterized by the projection m_j onto the field axis, and the corresponding eigenstates can be represented as $|(ns)jm_j\rangle$. For $n = 0$, $m_j = m_s$ and these states can alternatively be labeled by m_s.

The pattern is much more complicated when hyperfine interactions are included. In this case, the zero-field levels are labeled by the eigenvalues of the total angular momentum $\hat{f}$ resulting from coupling the nuclear spins $\hat{\imath}_{\rm N}$ and $\hat{\imath}_{\rm H}$ with $\hat{n}$ and $\hat{s}$. In general, three or more angular momenta can be coupled using a variety of schemes. We start, as before, by first coupling $\hat{n}$ and $\hat{s}$ to form $\hat{\jmath}$. Then, given the molecular constants in Table I, it is convenient to couple $\hat{\jmath}$ first with $\hat{\imath}_{\rm H}$ to produce a resultant $\hat{f}_{\rm H}$. Finally, $\hat{f}_{\rm H}$ is coupled with $\hat{\imath}_{\rm N}$ to give $\hat{f}$. In the particular case of $n = 0$, $j = s = 1$ and $f_{\rm H} = 1/2,3/2$, which produces levels with $f = 1/2$ and $3/2$ for $f_{\rm H} = 1/2$ and $f = 1/2$, $3/2$, and $5/2$ for $f_{\rm H} = 3/2$, as shown in Fig. 1. For $n = 0$, the Fermi contact terms make by far the largest contributions to the splittings, and levels with $f_{\rm H} = 3/2$ lie below those with $f_{\rm H} = 1/2$ because $b_{\rm F,H} < 0$. In a magnetic field, each f state further splits into $2f + 1$ sublevels, producing a total of $(2i_{\rm N} + 1)(2i_{\rm H} + 1)(2s + 1) = 18$ components correlating with the ground rotational state. At low fields, below about 10 G, the eigenfunctions are approximately represented as $|(ns)j,(ji_{\rm H})f_{\rm H},(f_{\rm H}i_{\rm N})fm_f\rangle$. In what follows, even though $f_{\rm H}$ and f are not good quantum numbers in a field, we use quantum numbers $(f_{\rm H},f,m_f)$ in parentheses to identify the states at low field. In addition, levels will be labeled β_i ($i = \overline{1,18}$) in order of increasing energy at fields above 50 G, where m_s is a nearly good quantum number. With this convention, β_1–β_6 correspond to $m_s = -1$, β_7–β_{12} to $m_s = 0$, and β_{13}–β_{18} to $m_s = +1$.

For isolated NH, the total projection m_f is a good quantum number. Hence, as a function of field, states corresponding to different m_f can cross while states of the same m_f cannot. However, in our model Hamiltonian, states β_{10} and β_{13} (both with $m_f = 1/2$) are seen to cross at about 25 G. This is a nonphysical effect which results from neglecting the interaction between the nuclear spins of N and H, usually

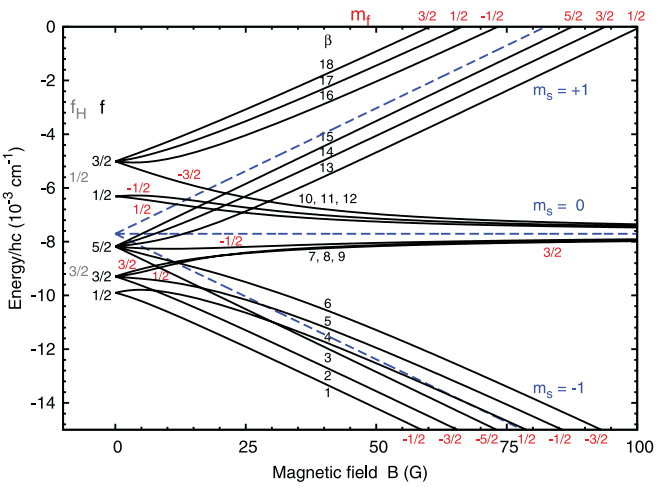

FIG. 1. (Color online) Magnetic-field dependence of the energy levels of ^{14}NH($^3\Sigma^-$) correlating with the ground rotational state, including (black, solid) and excluding (blue, dashed) hyperfine terms.

written in the form $c_4 \hat{i}_N \cdot \hat{i}_H$. For NH, c_4 is extremely small and has not been measured experimentally; there is in reality an avoided crossing between states β_{10} and β_{13}, but it is extremely tight.

At high field, the terms in the monomer Hamiltonian that mix states with different values of m_s are small with respect to the electron Zeeman splitting and m_s is well defined. For $n = 0$ at fields over 75 G, three groups of NH levels corresponding to $m_s = -1$, 0, and $+1$ can be identified, containing six hyperfine levels each. In this regime, the individual nuclear spin projections m_{iN} and m_{iH} are also nearly conserved, and the eigenfunctions are well represented by individual basis functions $|\alpha\rangle$. Above 75 G, more than 93.5% of any eigenstate is represented by a single basis function $|\alpha\rangle$. In the high-field limit we label states with quantum numbers in square brackets, $[m_s,m_{iN},m_{iH}]$.

All $m_s = +1$ states are low-field seeking and therefore trappable in a static magnetic trap. When hyperfine interactions are included, there are six such levels with different values of m_f. In contrast, when hyperfine terms are neglected, there is only one such state.

One state of particular interest is the *spin-stretched* state, in which f and m_f take their highest possible values. Except for terms off-diagonal in n, this state is exactly represented by a single basis function in either possible basis set, $(f_H, f, m_f) = (3/2,5/2, +5/2)$ or $[m_s,m_{iN},m_{iH}] = [+1, +1, +1/2]$. For ^{14}NH, the spin-stretched state is β_{15} and lies below three levels from the $(f_H, f) = (1/2,3/2)$ manifold, β_{16}–β_{18}.

B. Scattering cross sections

We have carried out scattering calculations using the MOLSCAT package [43], as modified to handle collisions in external fields [41]. The coupled equations were propagated with the hybrid log-derivative Airy method of Alexander and Manolopoulos [44], using a fixed-step-size log-derivative propagator for $2.5 \leqslant R \leqslant 50$ Å, with $\Delta R = 0.025$ Å, and a variable-step-size Airy propagator for $50 \leqslant R \leqslant 250$ Å. To a good approximation, the computer time is dominated by operations on relatively large matrices that scale with the total number of channels N as $\propto N^3$. The time needed to perform a calculation including hyperfine interactions is thus approximately $[(2i_N + 1)(2i_H + 1)]^3 = 216$ times larger than that required for an equivalent calculation neglecting them. In order to make our calculations tractable, the basis set used in the present work was reduced slightly from that used in Ref. [24], to $n_{max} = 5$ and $L_{max} = 6$. Under these conditions $N \approx 1500$, with the actual number depending on the initial state, M_{tot}, and P. The reduction in n_{max} and L_{max} does not change the results by more than about 5%.

NH molecules that undergo transitions between hyperfine levels of the $m_s = +1$ manifold remain in a magnetically trappable state. However, the associated kinetic energy release ranges from 0.7 to 5.8 mK and will either heat the trapped gas or eject one or both collision partners from the trap. We will thus assume that all inelastic processes have a negative impact on the success of sympathetic cooling. In any case, as will be shown in Sec. III B 3 a, transitions with $\Delta m_s = 0$ do not contribute appreciably to inelasticity.

1. General considerations

a. Analytical model. The total inelastic cross section may be decomposed into partial-wave contributions,

$$\sigma_{\beta,\text{inel}} = \sum_{\beta' \neq \beta, L, L'} \sigma_{\beta L \to \beta' L'}. \quad (16)$$

When inelastic scattering is weak compared to elastic scattering, the first-order distorted-wave Born approximation [45] provides relatively simple expressions for the off-diagonal S-matrix elements. Volpi and Bohn [46] gave an analytical formula for the threshold behavior of the partial inelastic cross sections under these conditions,

$$\sigma_{\beta L \to \beta' L'}(E,B) = \sigma_{\beta\beta'}^{LL'} E^{L-1/2} [E + \Delta E_{\beta\beta'}(B)]^{L'+1/2}. \quad (17)$$

Here, $\sigma_{\beta\beta'}^{LL'}$ is a factor independent of the collision energy E, while $\Delta E_{\beta\beta'}$ is the kinetic energy released in the transition from the state β to β'. This formula was used in interpreting the energy and magnetic-field dependence of hyperfine-free scattering cross sections in Mg + NH [24].

When hyperfine terms are neglected, $\Delta E_{\beta\beta'}$ in Eq. (17) is simply $-g_S \mu_B B \Delta m_s$ and $\sigma_{\beta\beta'}^{LL'}$ is independent of the magnetic-field strength B. However, when hyperfine terms are included, the B dependence of $\Delta E_{\beta\beta'}$ is much more intricate, as seen in Fig. 1. In particular, for many transitions, $\Delta E_{\beta\beta'}$ does *not* approach zero at low magnetic fields. This has substantial effects below about 50 G. At higher fields, $\Delta E_{\beta\beta'}$ approaches its hyperfine-free form even when hyperfine interactions are included. In addition, $\sigma_{\beta\beta'}^{LL'}$ varies with B because the character of the NH eigenstates depends on the magnetic field.

b. Relaxation mechanisms. The quantum-mechanical theory of electron spin relaxation in collisions of $^3\Sigma$ molecules with structureless atoms, neglecting hyperfine effects, was developed by Krems and Dalgarno [47]. In general, inelastic collisions are driven by the anisotropy of the interaction potential, but this does not have matrix elements that are off-diagonal in m_s. Collisions that change m_s thus occur only because it is not strictly a good quantum number, and basis functions with different values of m_s are mixed by terms in the monomer Hamiltonian. In the absence of hyperfine interactions, the only such terms are the spin-spin and spin-rotation Hamiltonians.

In the NH($^3\Sigma^-$) case that we study here, $\lambda_{ss} \gg \gamma$ and the electron spin-spin terms are dominant. There are no matrix elements of $\hat{\mathcal{H}}_{ss}$ between $n = 0$ states, because m_n cannot change from 0. In the absence of hyperfine interactions, the effect of $\hat{\mathcal{H}}_{ss}$ is to mix into the ground state $(m_s,n,m_n,M_L) = (m_s,0,0,M_L)$ a small amount of rotationally excited functions $(m_s - q,2,q,M_L)$ with $q = 0,\pm1,\pm2$. The potential anisotropy (principally V_2) can then drive transitions between these mixed states. Spin relaxation for $n = 0$ states thus proceeds mainly via the combination of the spin-spin interaction and the potential anisotropy, and leads to transitions with Δm_s compensated by a change in M_L to conserve M_{tot}. If $L = 0$, this requires $L' > 0$ and the corresponding cross sections are therefore *centrifugally suppressed* at low energies by barriers in the outgoing channels. In what follows, we will refer to this as the *main* relaxation mechanism.

When hyperfine coupling is included, states with different values of m_s and m_i are strongly mixed at low fields.

For the $n = 0$ states, this mixing is almost entirely due to the Fermi contact interactions. Under these circumstances the main mechanism can drive all possible transitions among the $n = 0$ states, although with varying degrees of centrifugal suppression as described below. However at high fields, once the Zeeman splittings are large compared to the Fermi contact interactions, m_s and m_i become nearly good quantum numbers. Since the main mechanism does not affect the nuclear spin projections, there is a propensity for transitions with $\Delta m_i = 0$.

2. *Dependence on collision energy*

Figure 2 shows the elastic and total inelastic cross sections as a function of energy at magnetic fields $B = 1$, 10, and 100 G, for collisions starting in the spin-stretched state, $\beta_{15} = (f_{\rm H}, f, m_f) = (3/2, 5/2, +5/2)$, and the two highest-lying states, $\beta_{17} = (1/2, 3/2, +1/2)$ and $\beta_{18} = (1/2, 3/2, +3/2)$. At very low energies, the scattering of incoming partial waves with $L \neq 0$ is suppressed by centrifugal barriers; our calculations include all contributions from incoming s, p, and d waves ($L = 0$ to 2), which gives integral cross sections that are converged at collision energies up to about 40 mK. The dashed lines in Fig. 2 show pure s-wave cross sections, and it may be seen that collisions with $L > 0$ become significant above $E \approx 10^{-4}$ K.

The dependence on the magnetic field will be analyzed in detail in the next section. However, in general terms it is clear that at high fields (100 G and above), the cross sections including hyperfine interactions are quite similar to those from hyperfine-free calculations, while at lower fields they are very different. In particular, the suppression of inelastic cross sections that occurs in hyperfine-free calculations at low fields and low energies is much reduced (resulting in larger inelastic cross sections) when hyperfine interactions are included.

The major effect of hyperfine interactions is that, at low fields, they increase the kinetic energy release and thus reduce the centrifugal suppression of the inelastic scattering. At 1 G, for example, the β_{17} and β_{18} states can relax to channels with kinetic energy releases of up to 7.2 mK, while the corresponding value for the spin-stretched β_{15} state is only 2.6 mK. When hyperfine coupling is excluded, however, the kinetic energy release at 1 G is only about 270 μK.

For simplicity, let us consider the case of s-wave scattering. The projection of the total angular momentum, $M_{\rm tot} = m_f + M_L$ (with $m_f = m_s + m_{i\rm N} + m_{i\rm H}$) is conserved in a collision, so $L' \geqslant |M'_L| = |\Delta m_f|$. In addition, conservation of parity requires L' to be even. For scattering from the spin-stretched state, β_{15}, the main relaxation channels have $m'_f = 1/2$ and 3/2, for which L' must be at least 2. Channels with $L' = 2$ dominate at low energies, because d-wave centrifugal barriers (height 23 mK) are much lower than g-wave barriers (height 140 mK). Transitions to levels for which $L' = 2$ is not possible, such as $(m'_f, L'_{\rm min}) = (-1/2,4),(-3/2,4),(-5/2,6)$, have negligible contributions at the energies and magnetic fields considered here.

For molecules that are initially in a non-spin-stretched state, inelastic collisions with $\Delta m_f = 0$ are possible. There are then relaxation channels with $L' = 0$, which are *not* centrifugally suppressed. However, transitions to these states are made possible only by invoking hyperfine couplings. Such transitions make very little contribution to the total inelastic cross section, which remains dominated by the (centrifugally suppressed) main mechanism. Even for molecules in non-spin-stretched states, the main effect of hyperfine interactions is through an increased kinetic energy release that helps overcome the centrifugal barriers at low fields and low energies.

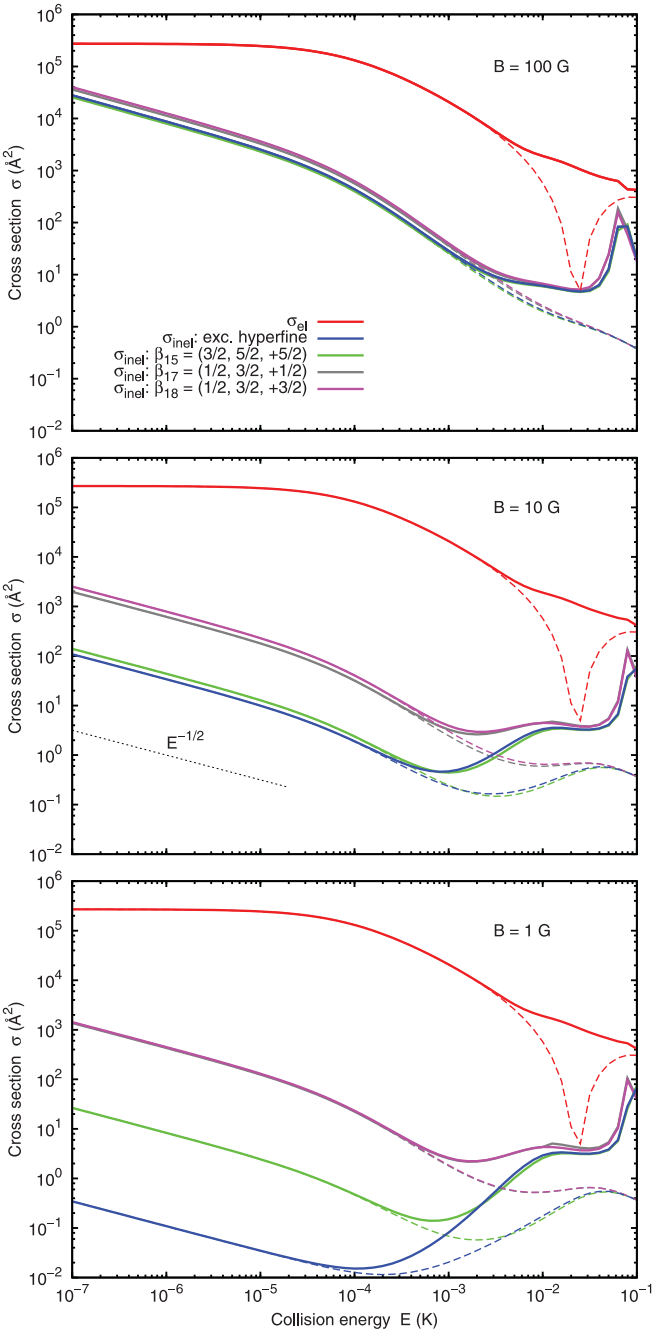

FIG. 2. (Color online) Elastic and total inelastic cross sections as a function of collision energy, for various magnetic fields and initial states. The elastic cross sections calculated with and without hyperfine terms are indistinguishable on the scale of the figure. Solid lines include s-, p- and d-wave contributions, while dashed lines are s-wave cross sections. The dotted line shows the power-law behavior as a guide to the eye.

In general, the elastic scattering depends on the phases of diagonal elements of the S matrix, which are only very slightly

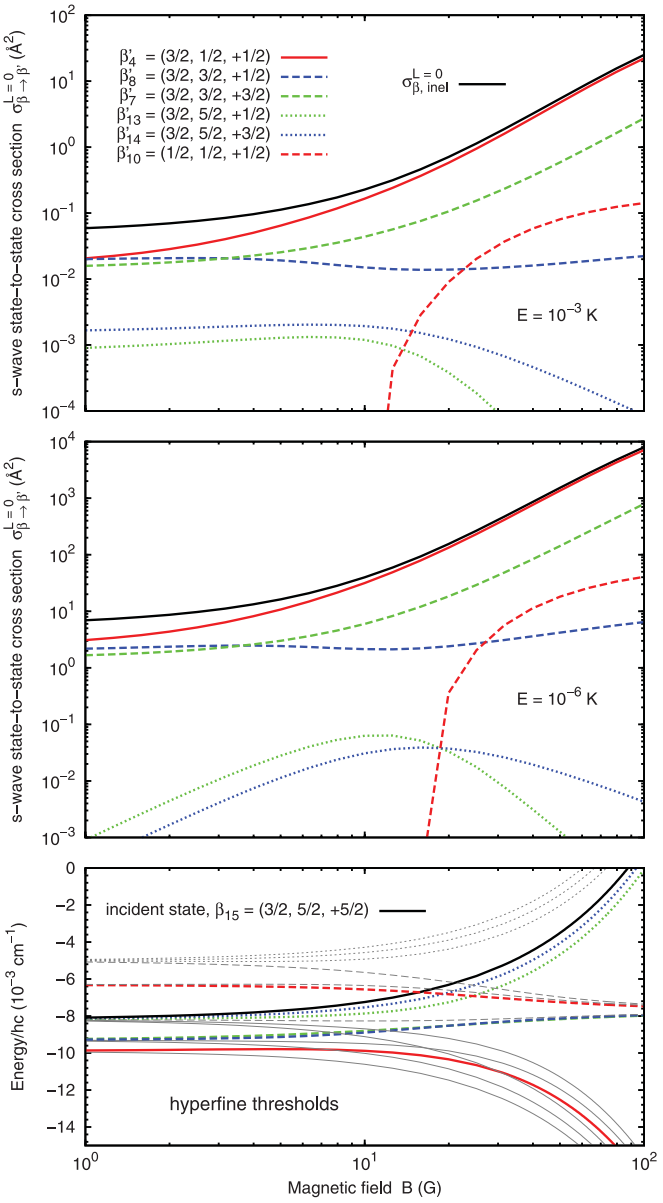

FIG. 3. (Color online) State-to-state s-wave inelastic cross sections for collisions originating in the spin-stretched state β_{15}, as a function of magnetic field, for collision energies of 10^{-3} K (top panel) and 10^{-6} K (center panel). The bottom panel shows the initial- and final-state energies, color coded as for the cross sections. Solid, dashed, and dotted lines represent states with $m_s = -1$, 0, and $+1$, respectively.

affected by the inclusion of hyperfine terms. The elastic cross sections including hyperfine interactions are very similar to the hyperfine-free results at all energies and fields and cannot be distinguished on the scale of Fig. 2.

3. *Dependence on magnetic field*

a. State-to-state s-wave cross sections. Figure 3 shows the state-to-state s-wave inelastic cross sections $\sigma^{L=0}_{\beta\to\beta'} \equiv \sum_{L'} \sigma_{0\beta\to L'\beta'}$ as a function of magnetic field B, for collisions starting in the spin-stretched state, β_{15}, with quantum numbers $(f_{\rm H}, f, m_f) = (3/2,5/2,+5/2)$ and $[m_s, m_{i\rm N}, m_{i\rm H}] = [+1,+1,+1/2]$. There are six main contributions, all to channels with $L' = 2$, corresponding to β'_4 ($\Delta m_s = -2$), β'_7, β'_8, and β'_{10} ($\Delta m_s = -1$), and β'_{13} and β'_{14} ($\Delta m_s = 0$). The corresponding final-state energies are shown color coded in the bottom panel.

At low fields, where the main mechanism can drive all possible transitions, the state-to-state cross sections are governed by the kinetic energy release. The largest cross section at $E = 10^{-6}$ K is to $\beta'_4 = (3/2,1/2,+1/2)$, closely followed by β'_7 and β'_8, which are $(3/2,3/2,+3/2)$ and $(3/2,3/2,+1/2)$, respectively. These channels have the largest kinetic energy release and therefore experience less centrifugal suppression. The relatively minor channels β'_{13} and β'_{14} have zero kinetic energy release at low field, while β'_{10} is energetically accessible only at fields above about 15 G (slightly dependent on E), as seen in the bottom panel.

At high fields, where m_s and m_i become nearly good quantum numbers, transitions with $\Delta m_i = 0$ are favored. The two strongest channels are $\beta'_4 = [-1,+1,+1/2]$ ($\sim$90%) and $\beta'_7 = [0,+1,+1/2]$ ($\sim$10%). The former is stronger because of the larger kinetic energy release associated with $\Delta m_s = -2$. The largest cross sections to channels with $\Delta m_i \neq 0$ are those to $\beta'_{10} = [0,+1,-1/2]$ and $\beta'_8 = [0,0,+1/2]$, with the former making a greater contribution because the Fermi contact interaction is stronger for H than for N. Transitions to $\beta'_{13} = [+1,-1,+1/2]$ and $\beta'_{14} = [+1,0,+1/2]$ are weak both because of the change in $m_{i,\rm N}$ and because they do not change m_s and thus have a small kinetic energy release.

The relative state-to-state cross sections are fairly insensitive to the collision energy, as seen by comparing the top and middle panels in Fig. 3. The only qualitative difference is in the cross sections to β'_{13} and β'_{14}, for which the kinetic energy release is zero at zero field. The inelasticity to these states is the most affected by centrifugal suppression. The outgoing kinetic energy for these channels is thus dominated by E, and the increase with collision energy at fields below $\sim$5 G is simply due to a larger probability of tunneling through the outgoing centrifugal barriers.

The behavior of the state-to-state cross sections from other states in the $m_s = +1$ manifold is considerably more complicated. Figure 4 shows the state-to-state cross sections for collisions that start in β_{18}, which at low field is $(1/2,3/2,+3/2)$ and at high field is $[+1,+1,-1/2]$. Once again the cross sections at low field are mostly governed by the kinetic energy release.

At high field, the strongest transitions are those to $\beta'_1 = [-1,+1,-1/2]$ and $\beta'_{10} = [0,+1,-1/2]$, which are driven by the main mechanism with no change in m_i quantum numbers. As before, the transition to $m_s = -1$ is stronger because of the larger kinetic energy release. The next strongest are to $\beta'_4 = [-1,+1,+1/2]$ and $\beta'_7 = [0,+1,+1/2]$, with $\Delta m_{i,\rm H} = +1$.

As discussed above, for non-spin-stretched states such as β_{18} it is possible to relax m_s while conserving m_f. This is the case for transitions to β'_7 and β'_{14}, which are dominated by $L' = 0$ and therefore are not centrifugally suppressed. However, it is clear from Fig. 4 that the centrifugally unsuppressed channels are not the dominant ones, even at very low field: the hyperfine splittings release enough kinetic energy that the main mechanism dominates over centrifugally unsuppressed transitions at all values of B.

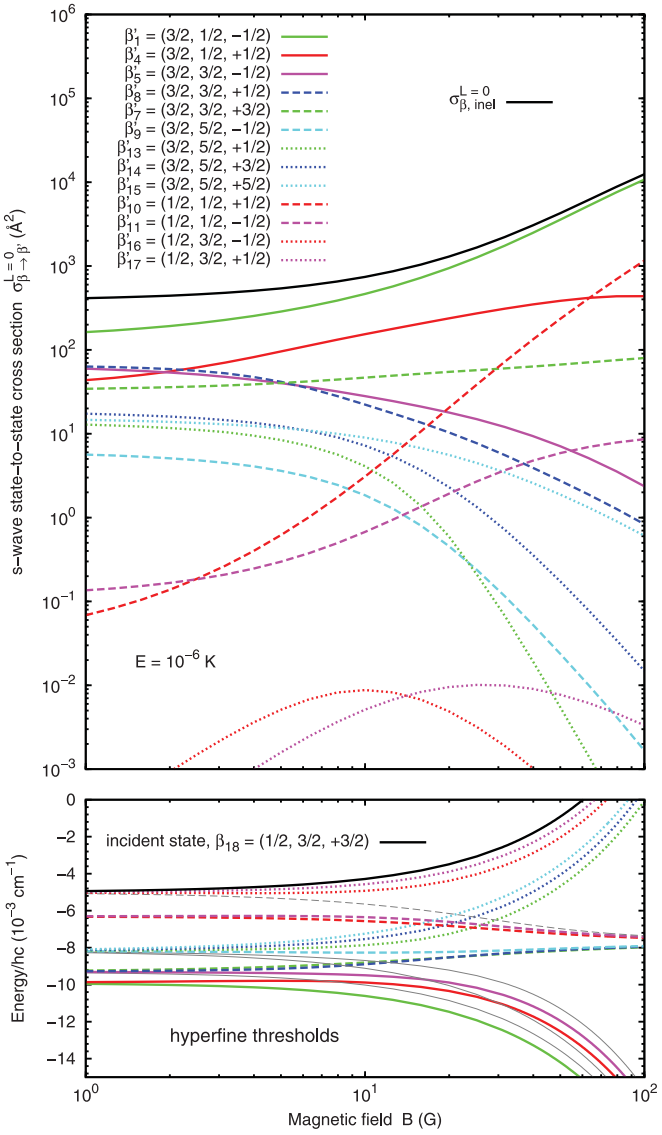

FIG. 4. (Color online) State-to-state s-wave inelastic cross sections for collisions originating in the uppermost hyperfine state, β_{18}, as a function of magnetic field, for a collision energy of 10^{-6} K (upper panel). The lower panel shows the initial and final states energies, color coded as for the cross sections. Solid, dashed, and dotted lines represent states with $m_s = -1$, 0, and +1, respectively.

b. Total s-wave inelastic cross sections. The behavior of the total s-wave inelastic cross sections with magnetic field, for the three initial states studied above, is shown in Fig. 5 for a range of collision energies. If hyperfine interactions are neglected, the quantity $\sigma^{0L'}_{\beta\beta'} \equiv \sigma^{0L'}_{m_s m'_s}$ of Eq. (17) is independent of B, $\Delta E_{\beta\beta'}$ is given by $-g_S \mu_B B \Delta m_s$, and three main regimes are observed [24]: (1) at low enough fields, the inelastic cross sections flatten out to a zero-field value proportional to E^2; (2) as the field increases, $\sigma^{L=0}_{\rm inel}$ enters a region of $B^{5/2}$ dependence, given by the increasing probability of tunneling through the d-wave centrifugal barrier in the dominant outgoing channel(s); and (3) at high enough fields (above about 100 G) the d-wave centrifugal barriers are overcome and $\sigma^{L=0}_{\rm inel}$ again approaches a field-independent value, this time proportional to $E^{-1/2}$.

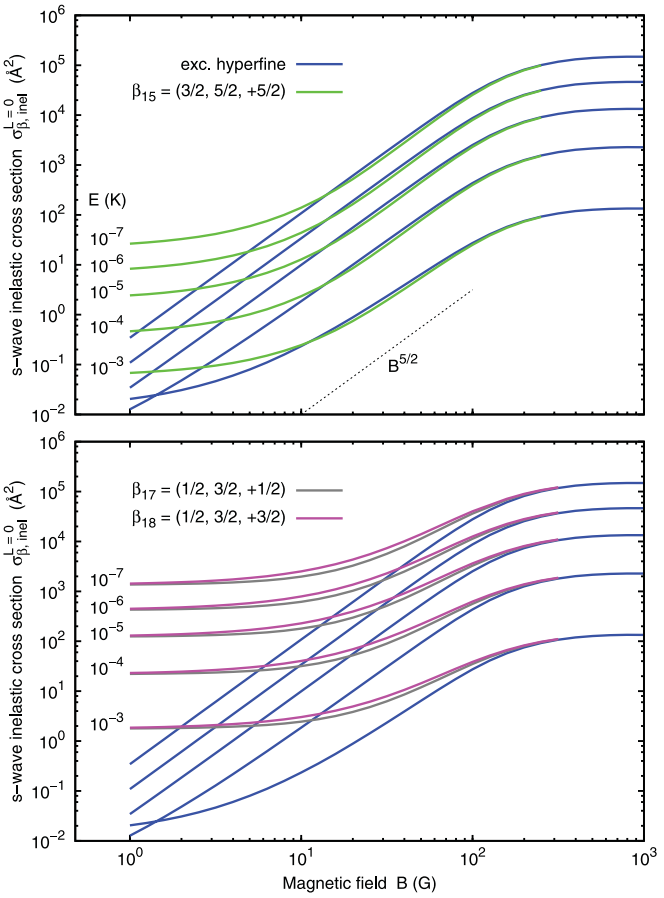

FIG. 5. (Color online) Total s-wave inelastic cross sections as a function of magnetic field for various collision energies and initial hyperfine states. The states are color coded as in Fig. 2. The dotted line shows the $B^{5/2}$ behavior in regime 2 (see text).

The inclusion of hyperfine terms modifies both the qualitative behavior in regime 1 and the boundaries of regime 2. First, at very low fields and collision energies, the state-to-state cross sections become nearly constant at a field-free value that is much larger than when hyperfine coupling is neglected. The kinetic energy release in this region is dominated by $\Delta E_{\beta\beta'}$, which for some outgoing channels does not approach zero as the field decreases. The field-free cross section is proportional to $E^{-1/2}$ at the lowest energies, although deviations from this occur at energies high enough that the outgoing energy is no longer dominated by $\Delta E_{\beta\beta'}$. Increasing the magnetic field alters $\Delta E_{\beta\beta'}$, particularly above ~10 G, but also changes $\sigma^{0L'}_{\beta\beta'}$ because the spin character of the monomer eigenfunctions changes. This leads to a non-power-law increase in the cross sections up to the onset of regime 2. It may again be noted that, although $L' = 0$ is possible for initial states other than the spin-stretched state, the hyperfine splitting at zero field provides enough kinetic energy release for the main mechanism to dominate spin relaxation, even though it is suppressed by d-wave outgoing barriers.

4. Prospects for sympathetic cooling

Trap losses in a static trap are fundamentally caused by four phenomena: spin relaxation, background gas collisions, blackbody radiation, and nonadiabatic transitions to

untrappable states. Nonadiabatic transitions, which are one-body transitions that can occur at points in the trap where different states are nearly degenerate, have important consequences for trap design. In particular, it is well known for atomic systems that substantial losses can occur at the center of magnetic quadrupole traps, where the magnetic field is zero [48]. Near this point, states with different values of m_f are degenerate and the trapping field varies very quickly with position, so that atoms can undergo nonadiabatic transitions (Majorana flops [49]) when they pass close to the trap center. For atoms, Majorana transitions can be effectively suppressed by applying a small bias field (1 G or less) that removes the zero-field point. Similar effects have been observed for molecules in electrostatic traps [50], and can again be suppressed by applying a bias field.

For molecules there are crossings that occur at nonzero field, as shown in Fig. 1. Magnetically trapped NH molecules in states β_{13}, β_{14}, and β_{15} might conceivably undergo transitions to untrapped states β_{10}, β_{11}, and β_{12} in the vicinity of crossings that occur between 15 and 30 G. However, away from the trap center the molecules experience a field that varies only slowly as they move, and under such circumstances the transition probabilities should be very low. We therefore expect that a small bias field of 1 G or less will be sufficient to suppress one-body losses for NH and other similar molecules. Even if such losses do prove significant, the states β_{16}, β_{17}, and β_{18} are immune to them except near a zero-field point.

The major loss mechanism in sympathetic cooling thus arises from inelastic collisions. Provided that the absolute values of the elastic cross sections are large enough to provide cooling before the molecules are lost to blackbody radiation or nonadiabatic transitions, the key quantity is the *ratio* of elastic to total inelastic cross sections, which must be greater than about 100 for sympathetic cooling to proceed.

Both Mg-NH and NH-NH [51,52] collisions may cause transitions to untrapped states or release enough energy to eject the molecules from the trap. Figure 6 shows contour plots of the ratio of elastic to total inelastic cross section as a function of E and B for Mg-NH. The top left panel shows the results when hyperfine terms are neglected, and the remainder show the results when hyperfine terms are included, for the spin-stretched and two highest-lying hyperfine states.

Trapped NH molecules in state β at temperature T will be distributed according to a Boltzmann distribution with density ρ given by

$$\rho/\rho_0 = \exp\left(\frac{E_\beta(0) - E_\beta(B)}{k_B T}\right). \tag{18}$$

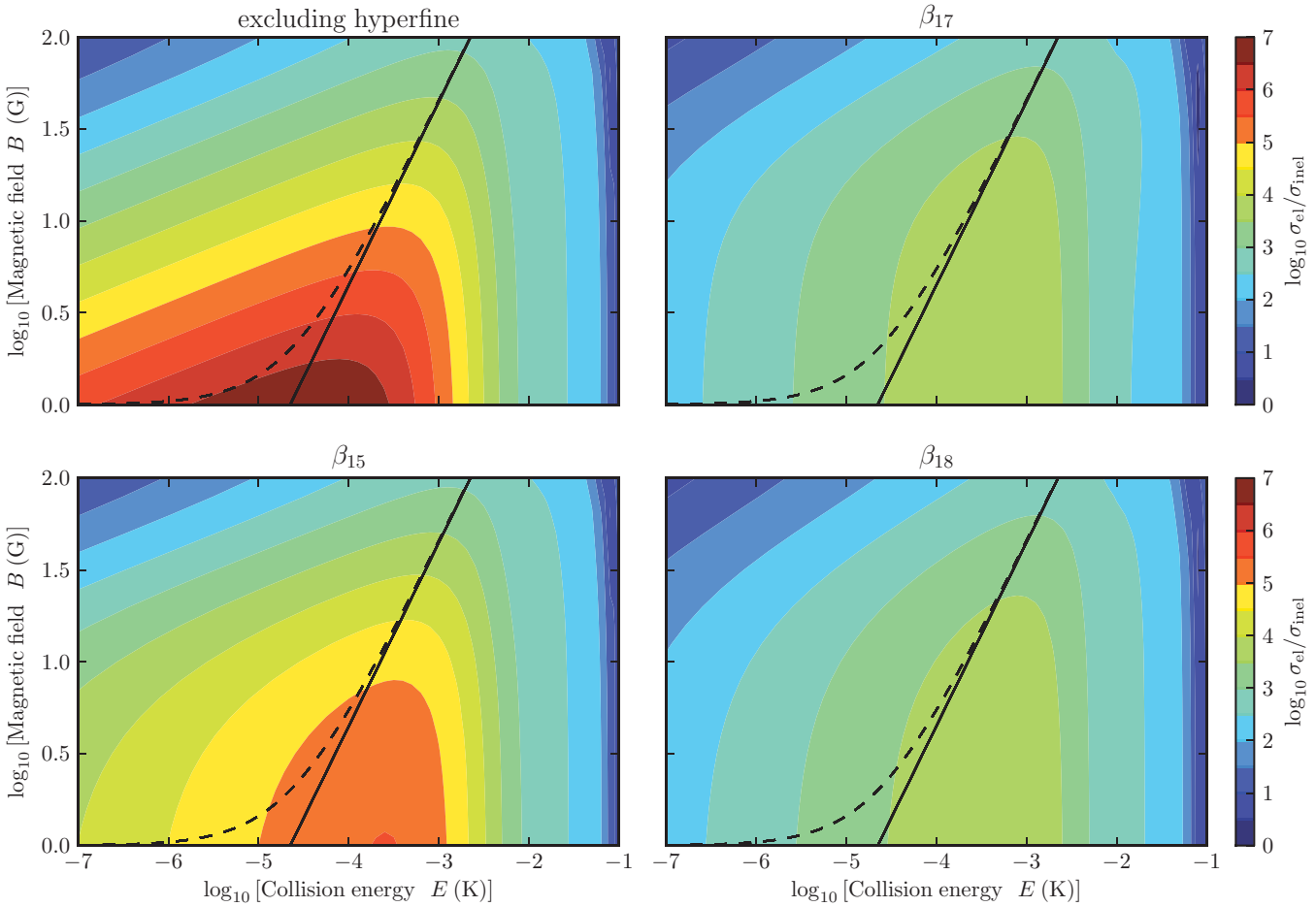

FIG. 6. (Color online) Contour plots of the ratio of elastic to total inelastic cross sections as a function of collision energy and magnetic field. The panels correspond to calculations excluding (top left) and including (the rest) hyperfine terms. The lines show the upper bound of the region sampled by over 99.9% of molecules trapped in the $m_s = +1$ state, in an unbiased trap (solid) and a trap with a bias field of $B = 1$ G (dashed).

At any given temperature on the energy axis of Fig. 6, only about 0.1% of molecules will experience fields corresponding to energies greater than $6k_BT$. The diagonal lines in Fig. 6 show the maximum fields sampled by over 99.9% of the molecules trapped in one of the hyperfine levels of the $m_s = +1$ manifold. These correspond, respectively, to an unbiased trap with zero magnetic field at the center (solid lines), and a trap with a bias field of 1 G, to prevent Majorana transitions (dashed lines). Precooled molecules will enter the trap from the right-hand side of the panels in Fig. 6 and then move to the left as they are cooled, remaining below the line appropriate for the trap in use.

The ratio of elastic to inelastic cross sections exceeds 100 at temperatures below 10 mK for all three hyperfine states, and is thus favorable for sympathetic cooling to work, provided the molecules can be precooled to this temperature. This agrees with the hyperfine-free results of Wallis and Hutson [24]. At lower temperatures and fields, the ratios of elastic to inelastic collisions are not as favorable as in hyperfine-free calculations, principally because of the increased kinetic energy release discussed above. Nevertheless, the ratios are adequate to reach temperatures below 1 μK. Trapping molecules in the fully spin-stretched state may be particularly advantageous, especially for molecules with stronger hyperfine interactions than NH.

IV. SUMMARY AND CONCLUSIONS

We have investigated the effect of hyperfine interactions on spin-relaxation collisions of NH with Mg in the cold and ultracold regimes. We find that hyperfine interactions make substantial changes to inelastic collision rates at temperatures below about 10 mK and magnetic fields below about 20 G. The major effect arises because hyperfine interactions modify the kinetic energy released in spin-relaxation collisions. When hyperfine interactions are neglected, the kinetic energy decreases to zero as the field is decreased, but when hyperfine interactions are included the kinetic energy release is significant for most transitions even at zero field. For s-wave collisions, the kinetic energy release helps overcome the d-wave centrifugal barriers that suppress spin-relaxation collisions and thus leads to larger inelastic cross sections.

Hyperfine interactions also introduce new mechanisms for spin-relaxation collisions. For initial states that are not spin-stretched, the cross sections for some of these are centrifugally unsuppressed. However, for Mg-NH, where the hyperfine interactions are quite weak, the centrifugally unsuppressed mechanisms make only a small contribution to total inelastic cross sections at the collision energies and fields studied here. It is nevertheless possible that centrifugally unsuppressed channels may be important in other systems, with either stronger hyperfine interactions or weaker competing spin-relaxation mechanisms.

The most important hyperfine effects for Mg-NH arise from the Fermi contact interactions. These determine both the composition of the $n = 0$ states in terms of spin functions and the low-field energy level pattern (and hence the kinetic energy release). Other hyperfine terms have only very small effects for transitions between $n = 0$ states. Indeed, we have repeated the calculations of the state-to-state cross sections including *only* the Fermi contact interactions and obtain almost identical results.

Our results for Mg-NH($^3\Sigma^-$) may be compared with those of Tscherbul *et al.* [34] for He-YbF($^2\Sigma$). For YbF the main mechanism of electron spin relaxation considered here, driven by the electron spin-spin coupling, does not exist and is replaced by a higher-order and much weaker mechanism driven by the spin-rotation interaction. Under these circumstances, combined electron and nuclear spin relaxation, driven by the electron-nuclear dipolar interaction, is in relative terms much more important. However, Tscherbul *et al.* did not focus on the regime where hyperfine energies make important contributions to the kinetic energy release.

We have considered the prospects for sympathetic cooling of NH by Mg, which were previously explored in hyperfine-free calculations by Wallis and Hutson [24]. We have calculated the ratio of the elastic to inelastic cross section as a function of energy and magnetic fields for several magnetically trappable hyperfine states of NH. Even though hyperfine interactions increase inelastic cross sections at low energies and magnetic fields, the ratio remains high enough for sympathetic cooling to proceed if the NH molecules can be precooled to about 10 mK.

Molecular hyperfine interactions are also likely to be important in developing techniques for controlling ultracold molecules. The low-lying excited states afforded by hyperfine splittings can support near-threshold levels that will produce magnetically tunable Feshbach resonances. Once molecules such as NH have been cooled to the ultracold regime, it will be possible to use such resonances both to control collisions by adjusting the scattering length and to create polyatomic molecules by magnetoassociation, as has already been achieved for alkali-metal atoms [13,14].

ACKNOWLEDGMENT

The authors are grateful to EPSRC for funding.

[1] L. D. Carr, D. DeMille, R. V. Krems, and J. Ye, New J. Phys. **11**, 055049 (2009).
[2] M. H. Anderson, J. R. Ensher, M. R. Matthews, C. E. Wieman, and E. A. Cornell, Science **269**, 198 (1995).
[3] C. C. Bradley, C. A. Sackett, J. J. Tollett, and R. G. Hulet, Phys. Rev. Lett. **75**, 1687 (1995).
[4] K. B. Davis, M. O. Mewes, M. R. Andrews, N. J. van Druten, D. S. Durfee, D. M. Kurn, and W. Ketterle, Phys. Rev. Lett. **75**, 3969 (1995).
[5] B. DeMarco and D. S. Jin, Science **285**, 1703 (1999).
[6] A. G. Truscott, K. E. Strecker, W. I. McAlexander, G. B. Partridge, and R. G. Hulet, Science **291**, 2570 (2001).

[7] J. D. Weinstein, R. deCarvalho, T. Guillet, B. Friedrich, and J. M. Doyle, Nature (London) **395**, 148 (1998).

[8] H. L. Bethlem and G. Meijer, Int. Rev. Phys. Chem. **22**, 73 (2003).

[9] N. Vanhaecke, U. Meier, M. Andrist, B. H. Meier, and F. Merkt, Phys. Rev. A **75**, 031402(R) (2007).

[10] S. D. Hogan, D. Sprecher, M. Andrist, N. Vanhaecke, and F. Merkt, Phys. Rev. A **76**, 023412 (2007).

[11] E. Narevicius, C. G. Parthey, A. Libson, J. Narevicius, I. Chavez, U. Even, and M. G. Raizen, New J. Phys. **9**, 358 (2007).

[12] E. S. Shuman, J. F. Barry, and D. DeMille, Nature (London) **467**, 820 (2010).

[13] J. M. Hutson and P. Soldán, Int. Rev. Phys. Chem. **25**, 497 (2006).

[14] T. Köhler, K. Góral, and P. S. Julienne, Rev. Mod. Phys. **78**, 1311 (2006).

[15] K. M. Jones, E. Tiesinga, P. D. Lett, and P. S. Julienne, Rev. Mod. Phys. **78**, 483 (2006).

[16] K. Bergmann, H. Theuer, and B. W. Shore, Rev. Mod. Phys. **70**, 1003 (1998).

[17] K.-K. Ni, S. Ospelkaus, M. H. G. de Miranda, A. Pe'er, B. Neyenhuis, J. J. Zirbel, S. Kotochigova, P. S. Julienne, D. S. Jin, and J. Ye, Science **322**, 231 (2008).

[18] J. Deiglmayr, A. Grochola, M. Repp, K. Mörtlbauer, C. Glück, J. Lange, O. Dulieu, R. Wester, and M. Weidemüller, Phys. Rev. Lett. **101**, 133004 (2008).

[19] J. G. Danzl, M. J. Mark, E. Haller, M. Gustavsson, R. Hart, J. Aldegunde, J. M. Hutson, and H.-C. Nägerl, Nature Phys. **6**, 265 (2010).

[20] *Cold Molecules: Theory, Experiment, Applications*, edited by R. V. Krems, B. Friedrich, and W. C. Stwalley (Taylor & Francis, London, 2009).

[21] C. J. Myatt, E. A. Burt, R. W. Ghrist, E. A. Cornell, and C. E. Wieman, Phys. Rev. Lett. **78**, 586 (1997).

[22] G. Modugno, G. Ferrari, G. Roati, R. J. Brecha, A. Simoni, and M. Inguscio, Science **294**, 1320 (2001).

[23] P. Soldán and J. M. Hutson, Phys. Rev. Lett. **92**, 163202 (2004).

[24] A. O. G. Wallis and J. M. Hutson, Phys. Rev. Lett. **103**, 183201 (2009).

[25] P. S. Żuchowski and J. M. Hutson, Phys. Chem. Chem. Phys. **13**, 3669 (2011).

[26] P. S. Żuchowski and J. M. Hutson, Phys. Rev. A **79**, 062708 (2009).

[27] T. V. Tscherbul, H.-G. Yu, and A. Dalgarno, Phys. Rev. Lett. **106**, 073201 (2011).

[28] H. L. Bethlem, G. Berden, F. M. H. Crompvoets, R. T. Jongma, A. J. A. van Roij, and G. Meijer, Nature (London) **406**, 491 (2000).

[29] R. deCarvalho, J. M. Doyle, B. Friedrich, T. Guillet, J. Kim, D. Patterson, and J. D. Weinstein, Eur. Phys. J. D **7**, 289 (1999).

[30] A. V. Avdeenkov and J. L. Bohn, Phys. Rev. A **66**, 052718 (2002).

[31] C. Ticknor and J. L. Bohn, Phys. Rev. A **71**, 022709 (2005).

[32] M. Lara, J. L. Bohn, D. Potter, P. Soldán, and J. M. Hutson, Phys. Rev. Lett. **97**, 183201 (2006).

[33] M. Lara, J. L. Bohn, D. E. Potter, P. Soldán, and J. M. Hutson, Phys. Rev. A **75**, 012704 (2007).

[34] T. V. Tscherbul, J. Kłos, L. Rajchel, and R. V. Krems, Phys. Rev. A **75**, 033416 (2007).

[35] P. Soldán, P. S. Żuchowski, and J. M. Hutson, Faraday Discuss. **142**, 191 (2009).

[36] J. M. Brown and A. Carrington, *Rotational Spectroscopy of Diatomic Molecules* (Cambridge University Press, Cambridge, 2003).

[37] R. A. Frosch and H. M. Foley, Phys. Rev. **88**, 1337 (1952).

[38] M. Mizushima, *Theory of Rotating Diatomic Molecules* (Wiley, New York, 1975).

[39] E. R. Cohen *et al.*, *Quantities, Units and Symbols in Physical Chemistry*, 3rd ed., IUPAC Green Book (IUPAC and RSC Publishing, Cambridge, 2008).

[40] J. Flores-Mijangos, J. M. Brown, F. Matsushima, H. Odashima, K. Takagi, L. R. Zink, and K. M. Evenson, J. Mol. Spectrosc. **225**, 189 (2004).

[41] M. L. González-Martínez and J. M. Hutson, Phys. Rev. A **75**, 022702 (2007).

[42] B. R. Johnson, J. Comput. Phys. **13**, 445 (1973).

[43] J. M. Hutson and S. Green, computer code MOLSCAT, version 14 (CCP6, Daresbury, 1994).

[44] M. H. Alexander and D. E. Manolopoulos, J. Chem. Phys. **86**, 2044 (1987).

[45] M. S. Child, *Molecular Collision Theory* (Academic Press, Oxford, 1974).

[46] A. Volpi and J. L. Bohn, Phys. Rev. A **65**, 052712 (2002).

[47] R. V. Krems and A. Dalgarno, J. Chem. Phys. **120**, 2296 (2004).

[48] W. Petrich, M. H. Anderson, J. R. Ensher, and E. A. Cornell, Phys. Rev. Lett. **74**, 3352 (1995).

[49] E. Majorana, Nuovo Cimento **9**, 43 (1932).

[50] M. Kirste, B. G. Sartakov, M. Schnell, and G. Meijer, Phys. Rev. A **79**, 051401(R) (2009).

[51] L. M. C. Janssen, P. S. Żuchowski, A. van der Avoird, G. C. Groenenboom, and J. M. Hutson, Phys. Rev. A **83**, 022713 (2011).

[52] L. M. C. Janssen, P. S. Żuchowski, A. van der Avoird, J. M. Hutson, and G. C. Groenenboom, J. Chem. Phys. **134**, 124309 (2011).